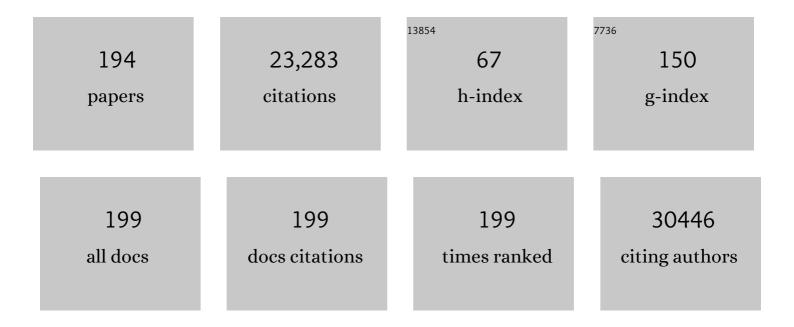
Chuan-Hong Jin

List of Publications by Year in descending order

Source: https://exaly.com/author-pdf/1842635/publications.pdf Version: 2024-02-01



#	Article	IF	CITATIONS
1	Large Scale Growth and Characterization of Atomic Hexagonal Boron Nitride Layers. Nano Letters, 2010, 10, 3209-3215.	4.5	2,317
2	Atomic layers of hybridized boron nitride and graphene domains. Nature Materials, 2010, 9, 430-435.	13.3	2,002
3	Perovskite light-emitting diodes based on solution-processed self-organized multiple quantum wells. Nature Photonics, 2016, 10, 699-704.	15.6	1,535
4	Exploring atomic defects in molybdenum disulphide monolayers. Nature Communications, 2015, 6, 6293.	5.8	1,124
5	Fabrication of a Freestanding Boron Nitride Single Layer and Its Defect Assignments. Physical Review Letters, 2009, 102, 195505.	2.9	973
6	Graphene Annealing: How Clean Can It Be?. Nano Letters, 2012, 12, 414-419.	4.5	801
7	Plasma-assisted fabrication of monolayer phosphorene and its Raman characterization. Nano Research, 2014, 7, 853-859.	5.8	606
8	Towards polyvalent ion batteries: A zinc-ion battery based on NASICON structured Na3V2(PO4)3. Nano Energy, 2016, 25, 211-217.	8.2	574
9	Deriving Carbon Atomic Chains from Graphene. Physical Review Letters, 2009, 102, 205501.	2.9	571
10	Highly active and durable methanol oxidation electrocatalyst based on the synergy of platinum–nickel hydroxide–graphene. Nature Communications, 2015, 6, 10035.	5.8	466
11	Interlayer couplings, Moiré patterns, and 2D electronic superlattices in MoS ₂ /WSe ₂ hetero-bilayers. Science Advances, 2017, 3, e1601459.	4.7	414
12	Growth of Largeâ€Area 2D MoS _{2(1â€<i>x</i>)} Se _{2<i>x</i>} Semiconductor Alloys. Advanced Materials, 2014, 26, 2648-2653.	11.1	347
13	Ultrasmall and phase-pure W2C nanoparticles for efficient electrocatalytic and photoelectrochemical hydrogen evolution. Nature Communications, 2016, 7, 13216.	5.8	334
14	Aligned, high-density semiconducting carbon nanotube arrays for high-performance electronics. Science, 2020, 368, 850-856.	6.0	308
15	Clean Transfer of Graphene for Isolation and Suspension. ACS Nano, 2011, 5, 2362-2368.	7.3	285
16	Epitaxy and Photoresponse of Two-Dimensional GaSe Crystals on Flexible Transparent Mica Sheets. ACS Nano, 2014, 8, 1485-1490.	7.3	285
17	Quantitative Analysis of Current–Voltage Characteristics of Semiconducting Nanowires: Decoupling of Contact Effects. Advanced Functional Materials, 2007, 17, 2478-2489.	7.8	283
18	Ultrastiff and Strong Graphene Fibers via Full‣cale Synergetic Defect Engineering. Advanced Materials, 2016, 28, 6449-6456.	11.1	279

#	Article	IF	CITATIONS
19	High Mobility 2D Palladium Diselenide Fieldâ€Effect Transistors with Tunable Ambipolar Characteristics. Advanced Materials, 2017, 29, 1602969.	11.1	251
20	Sulfur and Nitrogen Coâ€Đoped, Few‣ayered Graphene Oxide as a Highly Efficient Electrocatalyst for the Oxygenâ€Reduction Reaction. ChemSusChem, 2013, 6, 493-499.	3.6	242
21	Controlled Synthesis of High-Quality Monolayered α-In ₂ Se ₃ via Physical Vapor Deposition. Nano Letters, 2015, 15, 6400-6405.	4.5	239
22	Top–down fabrication of sub-nanometre semiconducting nanoribbons derived from molybdenum disulfide sheets. Nature Communications, 2013, 4, 1776.	5.8	220
23	Strong Local Coordination Structure Effects on Subnanometer PtO _{<i>x</i>} Clusters over CeO ₂ Nanowires Probed by Low-Temperature CO Oxidation. ACS Catalysis, 2015, 5, 5164-5173.	5.5	214
24	Atomic Defects in Twoâ€Ðimensional Materials: From Singleâ€Atom Spectroscopy to Functionalities in Optoâ€∤Electronics, Nanomagnetism, and Catalysis. Advanced Materials, 2017, 29, 1606434.	11.1	211
25	Two-Dimensional Molybdenum Tungsten Diselenide Alloys: Photoluminescence, Raman Scattering, and Electrical Transport. ACS Nano, 2014, 8, 7130-7137.	7.3	208
26	Stable Metallic 1Tâ€WS ₂ Nanoribbons Intercalated with Ammonia Ions: The Correlation between Structure and Electrical/Optical Properties. Advanced Materials, 2015, 27, 4837-4844.	11.1	207
27	Plumbing carbon nanotubes. Nature Nanotechnology, 2008, 3, 17-21.	15.6	202
28	Epitaxial Growth of Twinned Au–Pt Core–Shell Star-Shaped Decahedra as Highly Durable Electrocatalysts. Nano Letters, 2015, 15, 7808-7815.	4.5	195
29	Controlled Growth of Atomically Thin In ₂ Se ₃ Flakes by van der Waals Epitaxy. Journal of the American Chemical Society, 2013, 135, 13274-13277.	6.6	192
30	Direct growth of large-area graphene and boron nitride heterostructures by a co-segregation method. Nature Communications, 2015, 6, 6519.	5.8	190
31	Chemical vapor deposition growth of large-scale hexagonal boron nitride with controllable orientation. Nano Research, 2015, 8, 3164-3176.	5.8	171
32	Graphene Nanoribbons from Unzipped Carbon Nanotubes: Atomic Structures, Raman Spectroscopy, and Electrical Properties. Journal of the American Chemical Society, 2011, 133, 10394-10397.	6.6	170
33	General incorporation of diverse components inside metal-organic framework thin films at room temperature. Nature Communications, 2014, 5, 5532.	5.8	155
34	Tailoring the thermal and electrical transport properties of graphene films by grain size engineering. Nature Communications, 2017, 8, 14486.	5.8	154
35	Metalâ€Free Growth of Nanographene on Silicon Oxides for Transparent Conducting Applications. Advanced Functional Materials, 2012, 22, 2123-2128.	7.8	150
36	Fast Photoresponse from 1T Tin Diselenide Atomic Layers. Advanced Functional Materials, 2016, 26, 137-145.	7.8	150

#	Article	IF	CITATIONS
37	Reversible Conversion-Alloying of Sb ₂ O ₃ as a High-Capacity, High-Rate, and Durable Anode for Sodium Ion Batteries. ACS Applied Materials & Interfaces, 2014, 6, 19449-19455.	4.0	143
38	Engineering crystalline structures of two-dimensional MoS ₂ sheets for high-performance organic solar cells. Journal of Materials Chemistry A, 2014, 2, 7727-7733.	5.2	142
39	Kinetically controlled synthesis of Pt–Cu alloy concave nanocubes with high-index facets for methanol electro-oxidation. Chemical Communications, 2014, 50, 560-562.	2.2	140
40	High-Quality Ultralong Bi2S3 Nanowires:  Structure, Growth, and Properties. Journal of Physical Chemistry B, 2005, 109, 18772-18776.	1.2	137
41	TiS 2 nanoplates: A high-rate and stable electrode material for sodium ion batteries. Nano Energy, 2016, 20, 168-175.	8.2	137
42	Comparative Study on the Localized Surface Plasmon Resonance of Boron- and Phosphorus-Doped Silicon Nanocrystals. ACS Nano, 2015, 9, 378-386.	7.3	133
43	All Chemical Vapor Deposition Synthesis and Intrinsic Bandgap Observation of MoS ₂ /Graphene Heterostructures. Advanced Materials, 2015, 27, 7086-7092.	11.1	132
44	Robust Stacking-Independent Ultrafast Charge Transfer in MoS ₂ /WS ₂ Bilayers. ACS Nano, 2017, 11, 12020-12026.	7.3	130
45	Preparation of Singleâ€Layer MoS ₂ <i>_x</i> Se _{2(1â€} <i>_x</i> Se _{2(1â€} <i>_x</i> Se _x Mo <i>_x</i> Se ₂ Se ₂ Highâ€Concentration Metallic 1T Phase. Small. 2016. 12. 1866-1874.	5.2	126
46	Confinement of Perovskiteâ€QDs within a Single MOF Crystal for Significantly Enhanced Multiphoton Excited Luminescence. Advanced Materials, 2019, 31, e1806897.	11.1	124
47	Periodic Organic–Inorganic Halide Perovskite Microplatelet Arrays on Silicon Substrates for Roomâ€Temperature Lasing. Advanced Science, 2016, 3, 1600137.	5.6	121
48	In situ Study of Oxidative Etching of Palladium Nanocrystals by Liquid Cell Electron Microscopy. Nano Letters, 2014, 14, 3761-3765.	4.5	120
49	Capture the growth kinetics of CVD growth of two-dimensional MoS2. Npj 2D Materials and Applications, 2017, 1, .	3.9	115
50	Controlled Synthesis of Organic/Inorganic van der Waals Solid for Tunable Light–Matter Interactions. Advanced Materials, 2015, 27, 7800-7808.	11.1	109
51	Nanoporous core–shell Cu@Cu2O nanocomposites with superior photocatalytic properties towards the degradation of methyl orange. RSC Advances, 2012, 2, 12636.	1.7	104
52	Epitaxial Growth of Multimetallic Pd@PtM (M = Ni, Rh, Ru) Core–Shell Nanoplates Realized by in Situ-Produced CO from Interfacial Catalytic Reactions. Nano Letters, 2016, 16, 7999-8004.	4.5	103
53	Water-Assisted Preparation of High-Purity Semiconducting (14,4) Carbon Nanotubes. ACS Nano, 2017, 11, 186-193.	7.3	100
54	Strong interfacial coupling of MoS2/g-C3N4 van de Waals solids for highly active water reduction. Nano Energy, 2016, 27, 44-50.	8.2	96

#	Article	IF	CITATIONS
55	Van der Waals Epitaxial Growth of Atomic Layered HfS ₂ Crystals for Ultrasensitive Nearâ€Infrared Phototransistors. Advanced Materials, 2017, 29, 1700439.	11.1	96
56	Direct Chemical Vapor Deposition Growth and Band-Gap Characterization of MoS ₂ / <i>h</i> BN van der Waals Heterostructures on Au Foils. ACS Nano, 2017, 11, 4328-4336.	7.3	87
57	Phase Identification and Strong Second Harmonic Generation in Pure ε-InSe and Its Alloys. Nano Letters, 2019, 19, 2634-2640.	4.5	86
58	Amorphous oxygen-rich molybdenum oxysulfide Decorated p-type silicon microwire Arrays for efficient photoelectrochemical water reduction. Nano Energy, 2015, 16, 130-142.	8.2	85
59	One-Step Synthesis of Metal/Semiconductor Heterostructure NbS ₂ /MoS ₂ . Chemistry of Materials, 2018, 30, 4001-4007.	3.2	85
60	Ultrafine Nanoparticle‧upported Ru Nanoclusters with Ultrahigh Catalytic Activity. Small, 2015, 11, 4385-4393.	5.2	80
61	Vacancy Migrations in Carbon Nanotubes. Nano Letters, 2008, 8, 1127-1130.	4.5	79
62	Twoâ€Dimensional Layered Heterostructures Synthesized from Core–Shell Nanowires. Angewandte Chemie - International Edition, 2015, 54, 8957-8960.	7.2	78
63	Robust Phase Control through Hetero-Seeded Epitaxial Growth for Face-Centered Cubic Pt@Ru Nanotetrahedrons with Superior Hydrogen Electro-Oxidation Activity. Journal of Physical Chemistry C, 2015, 119, 17697-17706.	1.5	73
64	Anisotropic Spectroscopy and Electrical Properties of 2D ReS _{2(1–} <i>_x</i> ₎ Se ₂ <i>_x</i> Alloys with Distorted 1T Structure. Small, 2017, 13, 1603788.	5.2	70
65	Fabrication of MoSe2 nanoribbons via an unusual morphological phase transition. Nature Communications, 2017, 8, 15135.	5.8	70
66	Spatially-confined lithiation–delithiation in highly dense nanocomposite anodes towards advanced lithium-ion batteries. Energy and Environmental Science, 2015, 8, 1471-1479.	15.6	69
67	Colloidal Indium-Doped Zinc Oxide Nanocrystals with Tunable Work Function: Rational Synthesis and Optoelectronic Applications. Chemistry of Materials, 2014, 26, 5169-5178.	3.2	68
68	Boron- and Phosphorus-Hyperdoped Silicon Nanocrystals. Particle and Particle Systems Characterization, 2015, 32, 213-221.	1.2	68
69	Synthesis of in-plane and stacked graphene/hexagonal boron nitride heterostructures by combining with ion beam sputtering deposition and chemical vapor deposition. Nanoscale, 2015, 7, 16046-16053.	2.8	68
70	An In situ TEM study of the surface oxidation of palladium nanocrystals assisted by electron irradiation. Nanoscale, 2017, 9, 6327-6333.	2.8	68
71	In Situ Liquid Cell TEM Reveals Bridge-Induced Contact and Fusion of Au Nanocrystals in Aqueous Solution. Nano Letters, 2018, 18, 6551-6556.	4.5	68
72	Morphology Engineering in Monolayer MoS ₂ â€WS ₂ Lateral Heterostructures. Advanced Functional Materials, 2018, 28, 1801568.	7.8	67

#	Article	IF	CITATIONS
73	Controlled Growth and Reliable Thicknessâ€Dependent Properties of Organic–Inorganic Perovskite Platelet Crystal. Advanced Functional Materials, 2016, 26, 5263-5270.	7.8	64
74	Ultrathin Two-Dimensional Pd-Based Nanorings as Catalysts for Hydrogenation with High Activity and Stability. Small, 2015, 11, 4745-4752.	5.2	62
75	Growth of Polar Hexagonal Boron Nitride Monolayer on Nonpolar Copper with Unique Orientation. Small, 2016, 12, 3645-3650.	5.2	62
76	In-situ studies of electron field emission of single carbon nanotubes inside the TEM. Carbon, 2005, 43, 1026-1031.	5.4	61
77	Single-crystalline dendritic bimetallic and multimetallic nanocubes. Chemical Science, 2015, 6, 7122-7129.	3.7	61
78	NiS–MoS ₂ hetero-nanosheet array electrocatalysts for efficient overall water splitting. Sustainable Energy and Fuels, 2019, 3, 2056-2066.	2.5	61
79	In Situ Fabrication and Graphitization of Amorphous Carbon Nanowires and Their Electrical Properties. Journal of Physical Chemistry B, 2006, 110, 5423-5428.	1.2	60
80	Large-Scale Synthesis of Rings of Bundled Single-Walled Carbon Nanotubes by Floating Chemical Vapor Deposition. Advanced Materials, 2006, 18, 1817-1821.	11.1	57
81	Aligned Growth of Hexagonal Boron Nitride Monolayer on Germanium. Small, 2015, 11, 5375-5380.	5.2	56
82	Facile synthesis of Rh–Pd alloy nanodendrites as highly active and durable electrocatalysts for oxygen reduction reaction. Nanoscale, 2014, 6, 7012-7018.	2.8	55
83	Solventâ€Based Softâ€Patterning of Graphene Lateral Heterostructures for Broadband Highâ€Speed Metal–Semiconductor–Metal Photodetectors. Advanced Materials Technologies, 2017, 2, 1600241.	3.0	53
84	Inversion Domain Boundary Induced Stacking and Bandstructure Diversity in Bilayer MoSe ₂ . Nano Letters, 2017, 17, 6653-6660.	4.5	51
85	Atomic resolution liquid-cell transmission electron microscopy investigations of the dynamics of nanoparticles in ultrathin liquids. Chemical Communications, 2013, 49, 10944.	2.2	50
86	Fabrication of sub-nanometer pores on graphene membrane for ion selective transport. Nanoscale, 2018, 10, 5350-5357.	2.8	50
87	Black Phosphorus Quantum Dots Induced Highâ€Quality Perovskite Film for Efficient and Thermally Stable Planar Perovskite Solar Cells. Solar Rrl, 2019, 3, 1900132.	3.1	49
88	Highly active nanoporous Pt-based alloy as anode and cathode catalyst for direct methanol fuel cells. Journal of Power Sources, 2014, 267, 212-218.	4.0	48
89	Structural Phase Transition of Multilayer VSe ₂ . ACS Applied Materials & Interfaces, 2020, 12, 25143-25149.	4.0	47
90	In situ study of the growth of two-dimensional palladium dendritic nanostructures using liquid-cell electron microscopy. Chemical Communications, 2014, 50, 9447.	2.2	45

#	Article	IF	CITATIONS
91	Low-Temperature Growth of Two-Dimensional Layered Chalcogenide Crystals on Liquid. Nano Letters, 2016, 16, 2103-2107.	4.5	45
92	Probing the anisotropic behaviors of black phosphorus by transmission electron microscopy, angular-dependent Raman spectra, and electronic transport measurements. Applied Physics Letters, 2015, 107, .	1.5	44
93	NiS-MoS ₂ Hetero-nanosheet Arrays on Carbon Cloth for High-Performance Flexible Hybrid Energy Storage Devices. ACS Sustainable Chemistry and Engineering, 2019, 7, 11672-11681.	3.2	44
94	Revealing the Cluster loud and Its Role in Nanocrystallization. Advanced Materials, 2019, 31, e1808225.	11.1	41
95	Self-supporting nanoporous gold-palladium overlayer bifunctional catalysts toward oxygen reduction and evolution reactions. Nano Research, 2016, 9, 3781-3794.	5.8	39
96	Atomic Scale Stability of Tungsten–Cobalt Intermetallic Nanocrystals in Reactive Environment at High Temperature. Journal of the American Chemical Society, 2019, 141, 5871-5879.	6.6	39
97	Shaped Pt-Ni nanocrystals with an ultrathin Pt-enriched shell derived from one-pot hydrothermal synthesis as active electrocatalysts for oxygen reduction. Nano Research, 2015, 8, 1480-1496.	5.8	38
98	<i>In situ</i> electrical measurements of polytypic silver nanowires. Nanotechnology, 2008, 19, 085711.	1.3	36
99	Atomic process of oxidative etching in monolayer molybdenum disulfide. Science Bulletin, 2017, 62, 846-851.	4.3	36
100	Unveiling Growth Pathways of Multiply Twinned Gold Nanoparticles by <i>In Situ</i> Liquid Cell Transmission Electron Microscopy. ACS Nano, 2020, 14, 9594-9604.	7.3	36
101	Facile solvothermal synthesis of ultrathin LiFe _x Mn _{1â^x} PO ₄ nanoplates as advanced cathodes with long cycle life and superior rate capability. Journal of Materials Chemistry A, 2015, 3, 19368-19375.	5.2	35
102	Preparation of Twisted Bilayer Graphene via the Wetting Transfer Method. ACS Applied Materials & Interfaces, 2020, 12, 40958-40967.	4.0	35
103	Direct Imaging of Kinetic Pathways of Atomic Diffusion in Monolayer Molybdenum Disulfide. Nano Letters, 2017, 17, 3383-3390.	4.5	34
104	How Does A Carbon Nanotube Grow? An In Situ Investigation on the Cap Evolution. ACS Nano, 2008, 2, 1275-1279.	7.3	33
105	Boosting the performance of the Fe–N–C catalyst for the oxygen reduction reaction by introducing single-walled carbon nanohorns as branches on carbon fibers. Journal of Materials Chemistry A, 2019, 7, 23182-23190.	5.2	33
106	An improved Wiener deconvolution filter for high-resolution electron microscopy images. Micron, 2013, 50, 1-6.	1.1	32
107	Pt–Cu alloy with high density of surface Pt defects for efficient catalysis of breaking C–C bond in ethanol. Electrochimica Acta, 2014, 125, 29-37.	2.6	32
108	Layer-dependent anisotropic electronic structure of freestanding quasi-two-dimensional <mml:math xmlns:mml="http://www.w3.org/1998/Math/MathML"><mml:mrow><mml:mi>Mo</mml:mi><mml:msub><mml mathvariant="normal">S<mml:mn>2</mml:mn></mml </mml:msub></mml:mrow>. Physical Review B, 2016, 93, .</mml:math 	:mi 1.1	32

#	Article	IF	CITATIONS
109	In-situ fabrication of Mo6S6-nanowire-terminated edges in monolayer molybdenum disulfide. Nano Research, 2018, 11, 5849-5857.	5.8	32
110	Phase Separations in LiFe _{1–<i>x</i>} Mn _{<i>x</i>} PO ₄ : A Random Stack Model for Efficient Cathode Materials. Journal of Physical Chemistry C, 2014, 118, 796-803.	1.5	31
111	Kinetically-controlled growth of cubic and octahedral Rh–Pd alloy oxygen reduction electrocatalysts with high activity and durability. Nanoscale, 2015, 7, 301-307.	2.8	31
112	Black phosphorus nanoflakes as morphology modifier for efficient fullerene-free organic solar cells with high fill-factor and better morphological stability. Nano Research, 2019, 12, 777-783.	5.8	31
113	Formation of Subnanometer Zr-WOx Clusters within Mesoporous W–Zr Mixed Oxides as Strong Solid Acid Catalysts for Friedel–Crafts Alkylation. Journal of Physical Chemistry C, 2014, 118, 6283-6290.	1.5	30
114	Probing the oxidative etching induced dissolution of palladium nanocrystals in solution by liquid cell transmission electron microscopy. Micron, 2017, 97, 22-28.	1.1	28
115	Metal Atom Catalyzed Enlargement of Fullerenes. Physical Review Letters, 2008, 101, 176102.	2.9	27
116	Quantum Confined Tomonaga–Luttinger Liquid in Mo ₆ Se ₆ Nanowires Converted from an Epitaxial MoSe ₂ Monolayer. Nano Letters, 2020, 20, 2094-2099.	4.5	27
117	Deriving phosphorus atomic chains from few-layer black phosphorus. Nano Research, 2017, 10, 2519-2526.	5.8	26
118	Space-confined and substrate-directed synthesis of transition-metal dichalcogenide nanostructures with tunable dimensionality. Science Bulletin, 2020, 65, 1013-1021.	4.3	25
119	Highly Pure and Luminescent Graphene Quantum Dots on Silicon Directly Grown by Chemical Vapor Deposition. Particle and Particle Systems Characterization, 2016, 33, 8-14.	1.2	23
120	Deriving MoS ₂ nanoribbons from their flakes by chemical vapor deposition. Nanotechnology, 2019, 30, 255602.	1.3	22
121	Grain boundaries in chemical-vapor-deposited atomically thin hexagonal boron nitride. Physical Review Materials, 2019, 3, .	0.9	21
122	Performance change of few layer black phosphorus transistors in ambient. AIP Advances, 2015, 5, 107112.	0.6	20
123	Embedding Ultrafine and Highâ€Content Pt Nanoparticles at Ceria Surface for Enhanced Thermal Stability. Advanced Science, 2017, 4, 1700056.	5.6	20
124	Niobium doping induced mirror twin boundaries in MBE grown WSe2 monolayers. Nano Research, 2020, 13, 1889-1896.	5.8	20
125	High mobility top gated field-effect transistors and integrated circuits based on chemical vapor deposition-derived monolayer MoS ₂ . Materials Express, 2016, 6, 198-204.	0.2	19
126	Atomistic dynamics of sulfur-deficient high-symmetry grain boundaries in molybdenum disulfide. Nanoscale, 2017, 9, 10312-10320.	2.8	18

#	Article	IF	CITATIONS
127	Revealing the microscopic CVD growth mechanism of MoSe2 and the role of hydrogen gas during the growth procedure. Nanotechnology, 2018, 29, 314001.	1.3	18
128	Experimental study of protein translocation through MoS2 nanopores. Applied Physics Letters, 2019, 115, .	1.5	18
129	Characterization of Graphene Grown on Bulk and Thin Film Nickel. Langmuir, 2011, 27, 13748-13753.	1.6	17
130	Hydrogen-assisted post-growth substitution of tellurium into molybdenum disulfide monolayers with tunable compositions. Nanotechnology, 2018, 29, 145603.	1.3	17
131	Ion-templated fabrication of Pt-Cu alloy octahedra with controlled compositions for electrochemical detection of H2O2. Journal of Alloys and Compounds, 2019, 788, 1334-1340.	2.8	17
132	Efficiently producing single-walled carbon nanotube rings and investigation of their field emission properties. Nanotechnology, 2006, 17, 2355-2361.	1.3	16
133	Hole doping in epitaxial MoSe ₂ monolayer by nitrogen plasma treatment. 2D Materials, 2018, 5, 041005.	2.0	16
134	A Shallow Acceptor of Phosphorous Doped in MoSe ₂ Monolayer. Advanced Electronic Materials, 2020, 6, 1900830.	2.6	16
135	Deriving 2D M ₂ X ₃ (M = Mo, W, X = S, Se) by periodic assembly of chalcogen vacancy lines in their MX ₂ counterparts. Nanoscale, 2020, 12, 8285-8293.	2.8	16
136	Switching electron current in a semiconductor nanowire via controlling the carrier injection from the electrode. Applied Physics Letters, 2006, 89, 213108.	1.5	15
137	Direct evidence for lip-lip interactions in multi-walled carbon nanotubes. Nano Research, 2008, 1, 434-439.	5.8	15
138	Oxidation behavior of cobalt nanoparticles studied by in situ environmental transmission electron microscopy. Science Bulletin, 2017, 62, 775-778.	4.3	15
139	Interlayer Coupling Dependent Discrete H → T′ Phase Transition in Lithium Intercalated Bilayer Molybdenum Disulfide. ACS Nano, 2021, 15, 15039-15046.	7.3	15
140	Atomic-Precision Fabrication of Quasi-Full-Space Grain Boundaries in Two-Dimensional Hexagonal Boron Nitride. Nano Letters, 2019, 19, 8581-8589.	4.5	14
141	Understanding Anisotropic Growth of Au Penta-Twinned Nanorods by Liquid Cell Transmission Electron Microscopy. Journal of Physical Chemistry Letters, 2019, 10, 1443-1449.	2.1	14
142	Grain Boundary Motion in Two-Dimensional Hexagonal Boron Nitride. ACS Nano, 2020, 14, 13512-13523.	7.3	14
143	In Situ Formation and Structure Tailoring of Carbon Onions by High-Resolution Transmission Electron Microscopy. Journal of Physical Chemistry C, 2009, 113, 5043-5046.	1.5	13
144	Monolithic Integration of Vertical Thin-Film Transistors in Nanopores for Charge Sensing of Single Biomolecules. ACS Nano, 2021, 15, 9882-9889.	7.3	13

#	Article	IF	CITATIONS
145	Effective passivation of black phosphorus transistor against ambient degradation by an ultra-thin tin oxide film. Science Bulletin, 2019, 64, 570-574.	4.3	12
146	Magnetism in molybdenum disulphide monolayer with sulfur substituted by 3d transition metals. Journal of Applied Physics, 2016, 120, 144305.	1.1	11
147	Enhancing the production of hydrogen peroxide from electrocatalytic oxygen reduction reaction by tailoring the electronic states of single-walled carbon nanotubes: a synergistic effect from interior filling and exterior oxidation. Sustainable Energy and Fuels, 2019, 3, 1951-1956.	2.5	11
148	In situ transmission electron microscopy study of the formation and migration of vacancy defects in atomically thin black phosphorus. 2D Materials, 2021, 8, 025004.	2.0	11
149	Synthesis and Characterization of Ultrathin Tinâ€Doped Zinc Oxide Nanowires. European Journal of Inorganic Chemistry, 2012, 2012, 4268-4272.	1.0	10
150	Quantitative investigation of the formation and growth of palladium fractal nanocrystals by liquid-cell transmission electron microscopy. Chemical Communications, 2019, 55, 8186-8189.	2.2	10
151	The formation and shape transformation mechanism of a triangular Au nanoplate revealed by liquid-cell TEM. Nanoscale, 2020, 12, 19592-19596.	2.8	10
152	Selective Synthesis of Carbon Nanorings via Asymmetric Intramicellar Phase-Transition-Induced Tip-to-Tip Assembly. ACS Central Science, 2021, 7, 1493-1499.	5.3	10
153	Hf-Contacted High-Performance Air-Stable n-Type Carbon Nanotube Transistors. ACS Applied Electronic Materials, 2021, 3, 4623-4629.	2.0	10
154	Confinement effect induced conformation change of one-dimensional phosphorus chains filled in carbon nanotubes. Carbon, 2022, 189, 467-473.	5.4	10
155	Carbon Nanotube-Based Flexible Ferroelectric Synaptic Transistors for Neuromorphic Computing. ACS Applied Materials & Interfaces, 2022, 14, 30124-30132.	4.0	10
156	Design Synthesis of ITE Zeolite Using Nickel–Amine Complex as an Efficient Structure-Directing Agent. ACS Applied Materials & Interfaces, 2018, 10, 33214-33220.	4.0	9
157	In situ TEM study of edge reconstruction and evolution in monolayer black phosphorus. Nanoscale, 2021, 13, 4133-4139.	2.8	9
158	Single-layer Mo ₅ Te ₈ ― A new polymorph of layered transition-metal chalcogenide. 2D Materials, 2021, 8, 015006.	2.0	9
159	Semiconductors: Growth of Large-Area 2D MoS2(1-x) Se2x Semiconductor Alloys (Adv. Mater. 17/2014). Advanced Materials, 2014, 26, 2763-2763.	11.1	8
160	Multifarious Interfaces, Band Alignments, and Formation Asymmetry of WSe ₂ –MoSe ₂ Heterojunction Grown by Molecular-Beam Epitaxy. ACS Applied Materials & Interfaces, 2019, 11, 43766-43773.	4.0	8
161	Regulation of acidic properties of WO3-ZrO2 for Friedel–Crafts reaction with surfactant. Catalysis Communications, 2019, 123, 54-58.	1.6	8
162	Probing the degradation of carbon nanotubes in aqueous solution by liquid cell transmission electron microscopy. Carbon, 2019, 148, 481-486.	5.4	8

#	Article	IF	CITATIONS
163	Synergy between Structure Characteristics and the Solution Chemistry in a Near/Non-Equilibrium Oxidative Etching of Penta-Twinned Palladium Nanorods. Journal of Physical Chemistry C, 2021, 125, 4010-4020.	1.5	8
164	Mass transport induced structural evolution and healing of sulfur vacancy lines and Mo chain in monolayer MoS2. Rare Metals, 2022, 41, 333-341.	3.6	8
165	Study of intrinsic defect states of FeSe with scanning tunneling microscopy. Physical Review B, 2019, 100, .	1.1	7
166	Reversible H-T′ phase transition in monolayer molybdenum disulfide via electron beam assisted solid state lithiation/delithiation. Applied Physics Letters, 2020, 116, 033103.	1.5	7
167	Revealing the elemental-specific growth dynamics of Pt–Cu multipods by scanning transmission electron microscopy and chemical mapping. Journal of Materials Chemistry A, 2015, 3, 21284-21289.	5.2	6
168	Facile synthesis of hierarchical β-LiFePO4and its phase transformation to electrochemically active α-LiFePO4for Li-ion batteries. CrystEngComm, 2016, 18, 7707-7714.	1.3	6
169	Quantify point defects in monolayer tungsten diselenide. Nanotechnology, 2021, 32, 255701.	1.3	6
170	Revealing Au ₁₃ as Elementary Clusters During the Early Formation of Au Nanocrystals. Journal of Physical Chemistry Letters, 2021, 12, 5938-5943.	2.1	6
171	Direct identification of monolayer rhenium diselenide by an individual diffraction pattern. Nano Research, 2017, 10, 2535-2544.	5.8	5
172	Growth of â€~W' doped molybdenum disulfide on graphene transferred molybdenum substrate. Scientific Reports, 2018, 8, 7396.	1.6	5
173	Effects of non-rotationally symmetric aberrations on the quantitative measurement of lattice positions in a graphene monolayer using high-resolution transmission electron microscopy. Microscopy (Oxford, England), 2015, 64, 311-318.	0.7	4
174	Rapid-Heating-Triggered <i>in Situ</i> Solid-State Transformation of Amorphous TiO ₂ Nanotubes into Well-Defined Anatase Nanocrystals. Crystal Growth and Design, 2019, 19, 1086-1094.	1.4	4
175	Interactions of sub-five-nanometer diameter colloidal palladium nanoparticles in solution investigated <i>via</i> liquid cell transmission electron microscopy. RSC Advances, 2020, 10, 34781-34787.	1.7	4
176	Microdefect Characteristics in Castâ€Mono Silicon Wafers Induced by Slurry Sawing. Physica Status Solidi (A) Applications and Materials Science, 2021, 218, 2000258.	0.8	4
177	Post-synthesis Tellurium Doping Induced Mirror Twin Boundaries in Monolayer Molybdenum Disulfide. Applied Sciences (Switzerland), 2020, 10, 4758.	1.3	3
178	Probing the Controlled Oxidative Etching of Palladium Nanorods by Liquid Cell Transmission Electron Microscopy. Wuli Huaxue Xuebao/ Acta Physico - Chimica Sinica, 2019, 35, 15-21.	2.2	3
179	Modulation of electronic state in copper-intercalated 1T-TaS2. Nano Research, 2022, 15, 4327-4333.	5.8	3
180	Photodetectors: Solventâ€Based Softâ€Patterning of Graphene Lateral Heterostructures for Broadband Highâ€Speed Metal–Semiconductor–Metal Photodetectors (Adv. Mater. Technol. 2/2017). Advanced Materials Technologies, 2017, 2, .	3.0	2

#	Article	IF	CITATIONS
181	Spherical to truncated octahedral shape transformation of palladium nanocrystals driven by e-beam in aqueous solution. Nano Research, 2019, 12, 2623-2627.	5.8	2
182	Self-feeding formation of atomically thin molybdenum nanoflakes on MoS ₂ monolayer. 2D Materials, 2021, 8, 035054.	2.0	2
183	Surface Analysis of the Lithium-Rich Cathode Material Li _{1.2} Mn _{0.54} Co _{0.13} Ni _{0.13<!--<br-->by Advanced Electron Microscopy. Wuli Huaxue Xuebao/ Acta Physico - Chimica Sinica, 2016, 32, 2287-2292.}	sub>Na 2.2	a
184	In-Situ HR-TEM Characterizations on Individual Carbon Nanotubes During its Manipulation, Deformation and Growth. Microscopy and Microanalysis, 2009, 15, 710-711.	0.2	1
185	Inverse problem of the multislice method in retrieving projected complex potentials from the exit-wave function. Micron, 2014, 58, 47-54.	1.1	1
186	Graphene Quantum Dots: Highly Pure and Luminescent Graphene Quantum Dots on Silicon Directly Grown by Chemical Vapor Deposition (Part. Part. Syst. Charact. 1/2016). Particle and Particle Systems Characterization, 2016, 33, 2-2.	1.2	1
187	A microscopic TEM study of the defect layers in cast-mono crystalline silicon wafers induced by diamond-wire sawing. AIP Advances, 2021, 11, 045103.	0.6	1
188	Three-dimensional stacked filter (3DSF): a nonlinear filter for series images of TEM. Ultramicroscopy, 2022, 240, 113560.	0.8	1
189	B21-O-05Atomic motion in monolayer molybridenum disulfide probed by in-situ ADF-STEM. Microscopy (Oxford, England), 2015, 64, i41.2-i41.	0.7	0
190	Electron Microscopy Study of Surface Reconstruction and Its Evolution in P2-Type Na _{0.66} Mn _{0.675} Ni _{0.1625} Co _{0.1 for Sodium-Ion Batteries. Wuli Huaxue Xuebao/ Acta Physico - Chimica Sinica, 2016, 32, 1489-1494.}	1 62:5 </s	u b >O<
191	Three-leaf dart-shaped single-crystal BN formation promoted by surface oxygen. Applied Physics Letters, 2018, 113, 163101.	1.5	0
192	Small transition-metal dichalcogenide nanostructures down to subnanometer by two-dimensional material origami. Physical Review Materials, 2019, 3, .	0.9	0
193	Defect Physics in 2D Nanomaterials Explored by STEM/STM. , 2020, , 21-48.		0
194	Analysis of Single BSA Protein Molecules Using MoS ₂ Nanopores [*] ., 2022,,.		0

Analysis of Single BSA Protein Molecules Using MoS₂ Nanopores^{*}., 2022, , . 194